Interplane resistivity of underdoped single crystals $(Ba_{1-x}K_x)Fe_2As_2$ $(0 \leqslant x < 0.34)$

M. A. Tanatar,[1,2,*] W. E. Straszheim,[1] Hyunsoo Kim,[1,2] J. Murphy,[1,2] N. Spyrison,[1,2] E. C. Blomberg,[1,2] K. Cho,[1,2] J.-Ph. Reid,[3] Bing Shen,[4] Louis Taillefer,[3,5] Hai-Hu Wen,[4,6,5] and R. Prozorov[1,2]

[1]*Ames Laboratory, Ames, Iowa 50011, USA*

[2]*Department of Physics and Astronomy, Iowa State University, Ames, Iowa 50011, USA*

[3]*Département de Physique & RQMP, Université de Sherbrooke, Sherbrooke, Québec, Canada J1K 2R1*

[4]*Institute of Physics, Chinese Academy of Sciences, Beijing 100190, People's Republic of China*

[5]*Canadian Institute for Advanced Research, Toronto, Ontario, Canada M5G 1Z8*

[6]*National Laboratory of Solid State Microstructures and Department of Physics, Nanjing University, Nanjing 210093, People's Republic of China*

(Received 2 June 2011; revised manuscript received 11 April 2014; published 30 April 2014)

The temperature-dependent interplane resistivity $\rho_c(T)$ was measured in the hole-doped iron arsenide superconductor $(Ba_{1-x}K_x)Fe_2As_2$ over a doping range from parent compound to optimal doping at $T_c \approx 38$ K, $0 \leqslant x \leqslant 0.34$. The measurements were undertaken on high-quality single crystals grown from FeAs flux. The coupled magnetic/structural transition at T_{SM} leads to a clear accelerated decrease of $\rho_c(T)$ on cooling in samples with $T_c < 26$ K ($x < 0.25$). This decrease in the hole-doped material is in notable contrast to the increase in $\rho_c(T)$ in the electron-doped $Ba(Fe_{1-x}Co_x)Fe_2As_2$ and isoelectron-substituted $BaFe_2(As_{1-x}P_x)_2$. T_{SM} decreases very sharply with doping, dropping from $T_s = 71$ K to zero on increase of T_c from approximately 25 to 27 K. $\rho_c(T)$ becomes linear in T close to optimal doping. The broad crossover maximum in $\rho_c(T)$, found in the parent $BaFe_2As_2$ at around $T_{max} \sim 200$ K, shifts to higher temperature ~250 K with doping of $x = 0.34$. The maximum shows clear correlation with the broad crossover feature found in the temperature-dependent in-plane resistivity $\rho_a(T)$. The evolution with doping of T_{max} in $(Ba_{1-x}K_x)Fe_2As_2$ is in notable contrast with both the rapid suppression of T_{max} found in $Ba(Fe_{1-x}T_x)_2As_2$ (T = Co,Rh,Ni,Pd) and its rapid increase in $BaFe_2(As_{1-x}P_x)_2$. This observation suggests that pseudogap features are much stronger in hole-doped than in electron-doped iron-based superconductors, revealing significant electron-hole doping asymmetry similar to that in the cuprates.

DOI: 10.1103/PhysRevB.89.144514 PACS number(s): 74.70.Dd, 72.15.−v, 74.25.Jb

I. INTRODUCTION

Superconductivity in hole-doped $(Ba_{1-x}K_x)Fe_2As_2$ [1] (BaK122) was found soon after the discovery of superconductivity with high critical temperatures in oxypnictide FeAs-based materials [2]. Intensive studies of the doping phase diagram were undertaken on high-quality polycrystalline materials using neutron scattering, magnetization, heat capacity, and pressure-dependent measurements [3–6]. They revealed that as for electron doping in $Ba(Fe_{1-x}T_x)_2As_2$ [T = Co,Rh,Ni,Pd (BaT122)] [7] and isoelectron substitution in $BaFe_2(As_{1-x}P_x)_2$ [8] (BaP122), the maximum T_c is observed close to the point where magnetism vanishes, suggesting the possible existence of a quantum critical point (QCP) in the phase diagram [9,10] and magnetically mediated pairing [11,12].

A hallmark of this scenario is systematic evolution of the temperature-dependent resistivity $\rho(T)$ over the phase diagram. Typically $\rho(T)$ is close to being linear in T at optimum doping and to varying as T^2 in the overdoped regime [9,13], while at intermediate compositions it can be represented by either a power-law function $\rho(T) = \rho_0 + \rho_n T^n$ or as a sum of linear and quadratic terms, $\rho(T) = \rho_0 + \rho_1 T + \rho_2 T^2$. Interestingly, the magnitude of the T-linear contribution to the resistivity correlates with the superconducting T_c, providing an important link between anomalous scattering and pairing [13]. This doping-dependent $\rho(T)$ and a T-linear dependence at optimal doping are indeed observed in both in-plane, $\rho_a(T)$, and interplane, $\rho_c(T)$, resistivity of BaP122 [8,14], revealing clear signatures of a quantum critical point in both normal [10] and superconducting [15] states.

The situation is clearly more complicated in both electron-doped BaCo122 and hole-doped BaK122. In both cases the doping-dependent $T_N(x)$ was found to be nonmonotonic with reentrance of the tetragonal phase [4,16], suggesting no true existence of a quantum critical point in the phase diagram. Despite this, the in-plane transport in BaCo122 reveals systematic evolution from T-linear to T^2 dependence on going from optimal doping to overdoped compositions, as expected for the QCP scenario; however, the interplane resistivity $\rho_c(T)$ reveals T-linear dependence only in a narrow range above T_c, terminated at high temperatures by a broad crossover maximum at T_{max} [17,18]. A similar maximum is observed in $\rho_c(T)$ of all transition metal electron-doped compounds BaT122 [19]. By correlation with the T-linear increase of magnetic susceptibility and the NMR Knight shift, we related the maximum at T_{max} with a pseudogap [18], the existence of which was first suggested by NMR studies in electron-doped BaCo122 [20,21]. The pseudogap region extends from the parent compound to far beyond the end of the superconducting dome in the doping phase diagram for electron-doped BaCo122 [18,19]. The existence of a pseudogap in iron-based superconductors was later confirmed with spectroscopic [22,23] and angle-resolved photoemission spectroscopic (ARPES) [24] techniques.

The pseudogap is one of the dominant puzzling features in the phase diagram of the hole-doped cuprates [25]. On the other hand, its effect on the properties of electron-doped

*Corresponding author: tanatar@ameslab.gov

high-T_c cuprates is not so pronounced [26]. It has been suggested that the T-linear in-plane resistivity in the cuprates is determined by the quantum critical point of the pseudogap phase [27], and is linked with the competing nematic ordering [28]. These discussions strongly influence studies of the QCP scenario, nematicity, and the pseudogap in iron-based superconductors [29]. Previously, we have shown that electronic nematicity of the 122 family of iron-based superconductors is strongly suppressed on the hole-doped side of the phase diagram and even changes sign [30]. Therefore, it is of prime interest whether electron-hole doping asymmetry is also characteristic of the pseudogap features and QCP in iron pnictides. With this motivation in mind here we report a systematic study of the interplane (c-axis) transport in the hole-doped iron-based superconductor $(Ba_{1-x}K_x)Fe_2As_2$.

Previous studies of the doping evolution of the temperature-dependent in-plane resistivity in BaK122 [31,32] found that when the data are analyzed using a power-law function, $\rho(T) = \rho_0 + \rho_n T^n$, the exponent n of the fit monotonically decreases on approaching optimal doping from the underdoped side; however, it always remains higher than 1. Analysis of the frequency-dependent optical conductivity [33] of optimally doped BaK122 suggested that in fact the T-linear term in the resistivity is masked by the existence of two Drude contributions to the conductivity, only one of which is linear in T. A similar multicomponent analysis of conductivity was suggested by Golubov *et al.* [34] to explain the resistivity crossover at around 200 K. The authors considered a model in which two contributions to the conductivity have very different $\rho(T)$. One with low residual resistivity and strong T dependence dominates the low-temperature part of measured $\rho(T)$, while the one with high residual resistivity and weak T dependence becomes dominant at high temperatures. Alternatively the $\rho_a(T)$ of BaK122 was fitted by Gasparov *et al.* [35] using $\rho(T) = \rho_0 + \rho_n T^n + \rho_e \exp(-T_0/T)$, with the third term arising from phonon-assisted scattering between two Fermi-surface sheets.

Pressure studies of underdoped BaK122 crystals by Hassinger *et al.* [36] found an anomaly due to an intervening new phase in the doping range close to the compositional edge of magnetism, with an anomaly in in-plane transport of the crystals with $T_{SM} \sim 95$ K. An anomaly in a similar doping range was found at ambient pressure in the sign reversal of the in-plane resistivity anisotropy of BaK122 [30] and in high-quality polycrystalline samples of another hole-doped composition, BaNa122 [37].

As can be seen, there is no systematic picture of the evolution of the transport properties in hole-doped BaK122 on doping. An additional problem comes from the fact that properties of samples of BaK122 grown using different fluxes are different. The Sn-grown parent Ba122 shows quite significant suppression of T_{SM} down to 90 K [38], compared to approximately 135 K [7] in FeAs flux crystals or polycrystalline materials [1,4]. This strong suppression is ascribed to incorporation of Sn at subpercent level [39]. That is why the goal of this study is to characterize the evolution of the temperature-dependent resistivity on doping in high-quality single crystals of BaK122 grown from FeAs flux.

In this article we report a systematic study of the interplane resistivity of single crystals of BaK122, grown using the FeAs flux technique. Our main findings may be summarized as follows. (1) The pseudogap crossover maximum observed in $\rho_c(T)$ at $T_{\max}$ shifts moderately to higher temperatures as x increases in BaK122, significantly more slowly than it does in the isoelectron-substituted BaP122 [14] and with the opposite trend to that in electron-doped BaT122 [18,19]. (2) The crossover maximum correlates well with a slope-change feature in the temperature-dependent in-plane resistivity, suggesting its relation to carrier activation. (3) A range of T-linear dependence is observed in the interplane resistivity of BaK122 close to optimal doping, in contrast to the slightly superlinear dependence with $n = 1.1$ of the in-plane transport [32]. (4) The anomalies found in the pressure studies of the underdoped samples are not found reproducibly in the doping study, suggesting a difference between hole-doping and pressure-tuned phase diagrams.

II. EXPERIMENT

A. Sample preparation

Single crystals of BaK122 were grown using the high-temperature FeAs flux technique [31]. The volatility of K during growth leads to a distribution of the potassium content, with the inner parts of the crystals frequently having T_c differing by 1 to 3 K from the surface parts. Because of this distribution, as a first step in sample preparation for our study, we cleaved thin slabs from the inner parts of the crystals, typically of 20 μm thickness. The slabs had two clean and shiny cleavage surfaces. The samples were cleaved from these slabs with sides along the (100) directions using a razor blade. They typically had dimensions of $0.5 \times 0.5 \times 0.02\,\text{mm}^3$ ($a \times b \times c$).

We used two protocols for sample characterization for the interplane resistivity measurements. All samples were prescreened using a dipper version of the tunnel diode resonator (TDR) technique [40,41], using the sharpness of the superconducting transition as a measure of constant dopant concentration in each particular piece. These measurements also allowed us to exclude possible inclusions with lower T_c. After this prescreening, the samples with the sharpest transitions were characterized by a magneto-optical technique to look for possible inhomogeneity, as described in detail in Refs. [42–44], and then their chemical composition was determined using wavelength-dispersive x-ray spectroscopy (WDS) in a JEOL JXA-8200 electron microprobe. The composition was measured for 12 points per single crystal and averaged. We refer to this group of samples as group A in the following.

The interplane resistivity was measured on all crystals studied by WDS to determine the resistive T_c and the structural transition temperature T_{SM} as functions of composition x. For this purpose the top and bottom surfaces of the samples were covered with Sn solder [44,45] and 50 μm silver wires were attached to enable measurements in the four-probe configuration. Soldering produced contacts with resistance typically in the 10 $\mu\Omega$ range. The interplane resistivity was measured using a two-probe technique with currents in the 1 to 10 mA range (depending on the sample resistance, which is typically 1 mΩ), relying on the negligibly small contact resistance. The four-probe scheme was used on the

sample to measure the series-connected sample, R_s, and contact, R_c, resistance. Taking into account that $R_s \gg R_c$, the contact resistance represents a minor correction of the order of 1% to 5%. This can be directly seen for our samples for temperatures below the superconducting T_c, where $R_s = 0$ and the measured resistance represents R_c [17,42,44]. The details of the measurement procedure can be found in Refs. [17,18,46].

The drawback of the measurement on samples with $c \ll a$ is that any inhomogeneity in the contact resistance or internal sample connectivity mixes in the in-plane component due to redistribution of the current. This requires measurements on a bigger array of samples, beyond our possibility of WDS measurements. To check for reproducibility, we performed ρ_c measurements on samples which had same dipper TDR T_c as samples of group A. We refer to these samples as group B. We performed measurements of ρ_c on at least five samples of each batch with the same dipper TDR T_c; at least one of the samples was measured by WDS to determine composition. In all cases we obtained qualitatively similar temperature dependencies of the electrical resistivity, as represented by the ratio of resistivities at room and low temperatures, $\rho_c(0)/\rho_c(300)$. The resistivity value, however, showed a notable scatter and at room temperature, $\rho_c(300\ \mathrm{K})$, was typically in the range 1000 to 2000 $\mu\Omega$ cm.

Because $\rho_c(T)$ measurements are made in the two-probe mode, the resistivity value below T_c is always finite and represents the contact resistance. Therefore the superconductive transition temperature was determined as an offset point of the sharp part of the resistive transition, as shown in Fig. 1. For reference we show in the same graph the temperature-dependent TDR frequency shift of the same sample before contact application. We find that the offset point of the superconducting transition in $\rho_c(T)$ measurements corresponds well to the onset point in $\Delta f(T)$. In the right panel of Fig. 1 we show the temperature-dependent interplane resistivity of the same sample in the temperature range of the structural/magnetic transition. We also show the temperature dependence of the resistivity derivative $d[\rho_c(T)/\rho_c(300\ \mathrm{K})]/dT$. It is of note that,

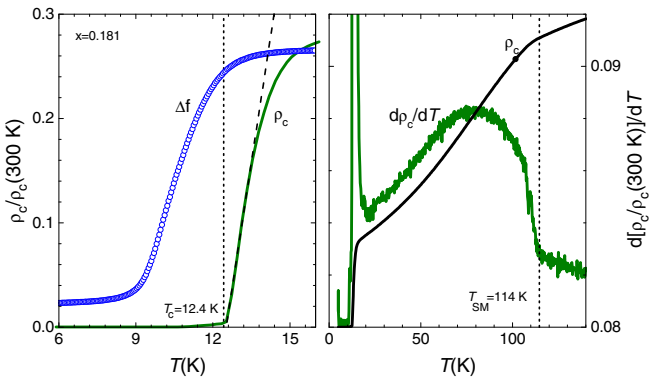

FIG. 1. (Color online) Left panel: Temperature-dependent resistivity and frequency shift in TDR measurements (shown in arbitrary units) in the superconducting transition range, used to determine the superconducting T_c of samples of group A. Right panel: a zoom of the $\rho_c(T)$ in the area of the structural transition (arbitrary scale), showing the criterion used to determine T_{SM}.

in contrast to the in-plane resistivity, the structural/magnetic transition leads to a resistivity decrease and onset of an increase of the resistivity derivative. We define T_{SM} as the onset point of rapid rise in $d[\rho_c(T)/\rho_c(300\ \mathrm{K})]/dT$. Note that the resistivity derivative has a singular feature at the transition, in contrast to the split double-feature structure observed in BaCo122 [7]. This is consistent with the coincident tetragonal-to-orthorhombic and antiferromagnetic transitions found in neutron scattering experiments [4].

III. RESULTS

A. WDS composition analysis

In Fig. 2 we show the evolution of the temperatures of the structural/magnetic and superconducting transitions in the crystals of group A. For reference we show data obtained on high-quality polycrystalline materials, and in the previous study on single crystals [31]. The three studies are in reasonable agreement with the minor difference being in determinations at the very edge of the superconducting dome. Our study suggests that superconductivity sets in at $x = 0.15$, which is somewhat higher than the value found by Avci *et al.* [4].

The doping evolution of the structural transition temperature T_{SM} is in reasonable agreement with neutron scattering data of Avci *et al.* [4]. The fit of $T_{SM}(x)$ requires a third-order polynomial and is not very precise. It is of note that, despite quite small steps in T_c of the samples, we have not found samples with structural transition temperatures below 71 K, which may suggest a very sharp termination of $T_{SM}(x)$.

The dependence of the zero-resistivity T_c can be well fitted over the range studied using a parabolic function, $T_c = 38.5 - 54(0.345 - x) - 690(0.345 - x)^2$, as shown by the solid line. This parabolic dependence is similar to the parabolic dependence found in the cuprates [47]. In contrast to the cuprates, though, this dependence is very asymmetric in BaK122 [1,4]; it obviously fails in the overdoped regime.

The samples shown in the top panel of Fig. 2 have a monotonic relation between T_c and T_{SM}, similar to the behavior found in previous studies on BaK122 polycrystals [1,4,5] and for other doping types [7,48–50]. This dependence provides an intrinsic check for sample quality and is shown in the bottom panel of Fig. 2 with solid dots. This monotonic dependence is in striking contrast with the measurements under pressure by Hassinger *et al.* [36], finding a competing phase reducing T_c from its trend with doping, which thus should lead to an anomaly in $T_c(T_N)$. This observation is suggestive that the doping and pressure phase diagrams are not quite equivalent in the BaK122 system, This unusual difference of the two tuning parameters is not found in electron-doped BaCo122 [51], in which pressure and doping lead to similar T_c evolution. It is also different from the behavior in isoelectron-substituted BaRu122 [52]. In contrast, a difference between doping and pressure tuning was found in thin films of indirectly electron-doped BaLa122 [53], in which T_c monotonically increases with pressure in both the underdoped and overdoped regimes.

B. Maximum of the interplane resistivity

In Fig. 3 we show the evolution with doping of the temperature-dependent interplane resistivity in BaK122. In

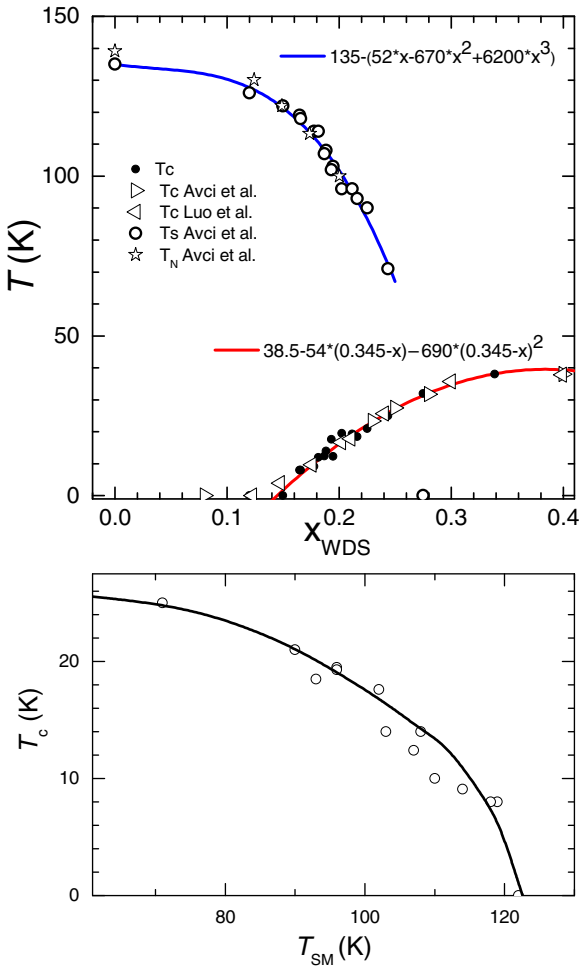

FIG. 2. (Color online) Top panel: The structural/magnetic transition temperature T_{SM} (open circles) and the superconducting T_c (solid circles) as functions of x determined in WDS measurements on the same crystals of group A. The definitions of T_c and T_{SM} are shown in Fig. 1. For reference we show $T_c(x)$ (right open triangles) as determined from magnetization measurements and $T_{SM}(x)$ (open stars) as determined from neutron scattering measurements on high-quality polycrystalline samples, [4,5] and $T_c(x)$ as determined from resistivity measurements (open left triangles) on single crystals grown out of FeAs flux [31]. The lines show fits through the data for $T_{SM}(x)$ (blue) and $T_c(x)$ (red) curves. Bottom panel: $T_c(T_N)$ dependence, as determined in our measurements on the same crystals. This dependence is monotonic, suggesting no doping anomaly in either T_c or T_N.

addition to features due to the magnetic/structural transition at T_{SM} and superconductivity at T_c, discussed above, $\rho_c(T)$ shows a clear maximum, observed in the parent Ba122 at $T_{\max} \approx 200$ K. Because of the broad crossover character and a possible influence on the position of the maximum of the admixture of $\rho_a(T)$ [17], the maximum is defined with rather large error bars of about ± 20 K. The doping up to $x = 0.235$, on the edge of the orthorhombic/antiferromagnetic domain in the phase diagram, does not change the position of the maximum within the error bars; doping to $x = 0.34$, close to optimal doping, slightly shifts $T_{\max}$ to higher temperatures.

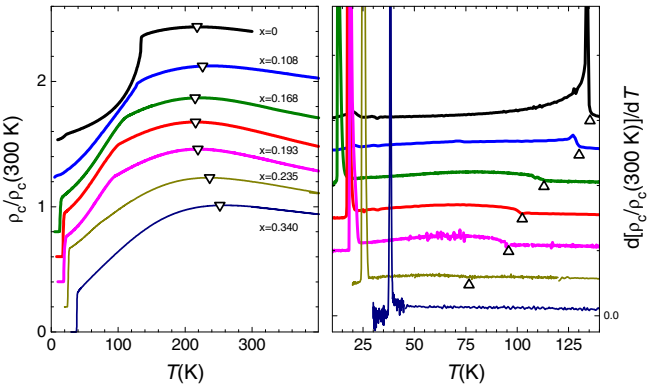

FIG. 3. (Color online) Left panel: Doping evolution of the temperature-dependent inter-plane resistivity $\rho_c(T)$, normalized to room temperature values $\rho_c(300\ \mathrm{K})$. The curves are offset to avoid overlapping. Down triangles show the position of the $\rho_c(T)$ maximum at $T_{\max}$. Right panel: Temperature-dependent resistivity derivative, with up triangles showing the position of T_{SM}.

IV. DISCUSSION

A. Structural/magnetic ordering and interplane resistivity

In contrast to BaCo122 and BaP122, stripe antiferromagnetic ordering and the tetragonal-to-orthorhombic structural transition happen simultaneously in BaK122 at a temperature $T_{SM} = T_{TO} = T_N$ [4,5]. Magnetic ordering reconstructs the Fermi surface, opening nesting or superzone gaps in electron and hole pockets [54]. In hole-doped materials this gap opening, instead of leading to a resistivity increase, leads to an accelerated resistivity decrease (increase of the resistivity derivative), suggesting that the main effect comes from a change in the inelastic scattering due to decrease of the contribution of pretransition fluctuations of the order parameter. The parts of the Fermi surface which are not affected by the spin-density wave (SDW) gap [30,54] enjoy a notably reduced inelastic scattering in the magnetically ordered phase [30,55–58]. The disorder inevitably accompanying random distribution of dopant atoms increases the residual resistivity of the compounds. This doping disorder is absent in the parent compound, so that decrease of inelastic scattering overcomes the loss of the carrier density and the total conductivity increases below T_{SM}. Since the interplane transport is dominated by the most warped parts of the Fermi surface [17], least affected by the SDW superzone gap, the interplane resistivity should be affected much less by the SDW gap opening than ρ_a. This is indeed seen in BaK122, very much as in BaCo122.

The response of $\rho_c(T)$ to the structural/magnetic transition is distinctly different for hole-doped BaK122, electron-doped BaCo122, and isoelectron-substituted BaP122. In Fig. 4 we compare $\rho_c(T)$ for these different types of doping for compositions with transition temperatures of the order of 100 K, $x = 0.19$ in $(Ba_{1-x}K_x)Fe_2As_2$ (top panel), $x = 0.23$ in $BaFe_2(As_{1-x}P_x)_2$ (middle panel), and $x = 0.038$ in $Ba(Fe_{1-x}Co_x)_2As_2$. The rise of ρ_c in relative units is largest in BaCo122, and smallest (zero) in BaK122, following the same trend as the maximum T_c in the series. The comparison of the three curves at high temperatures gives a direct hint

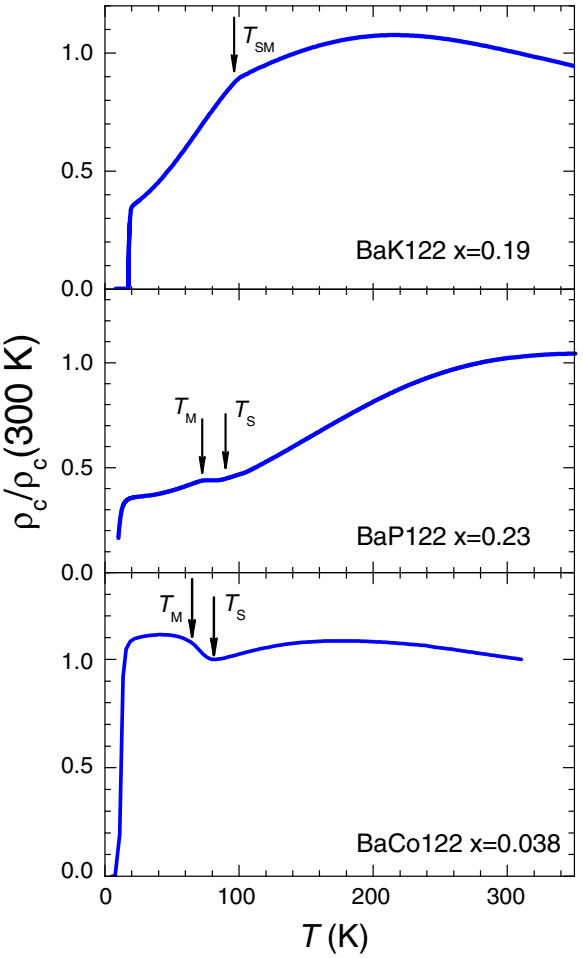

FIG. 4. (Color online) Temperature-dependent interplane resistivity of underdoped samples of Ba122-based superconductors. Top panel: hole-doped $(Ba_{1-x}K_x)Fe_2As_2$, $x = 0.19$. Middle panel: isoelectron-substituted $BaFe_2(As_{1-x}P_x)_2$, $x = 0.23$. Bottom panel: electron-doped $Ba(Fe_{1-x}Co_x)_2As_2$, $x = 0.038$. The resistivity rises significantly below T_S in BaCo122, with a small slope change at T_N; the decrease is smaller in BaP122 and is absent in BaK122. Comparison of the three curves also illustrates the different evolution with doping of T_{max} for the three different types of doping; see the phase diagram of the feature in Fig. 5 below.

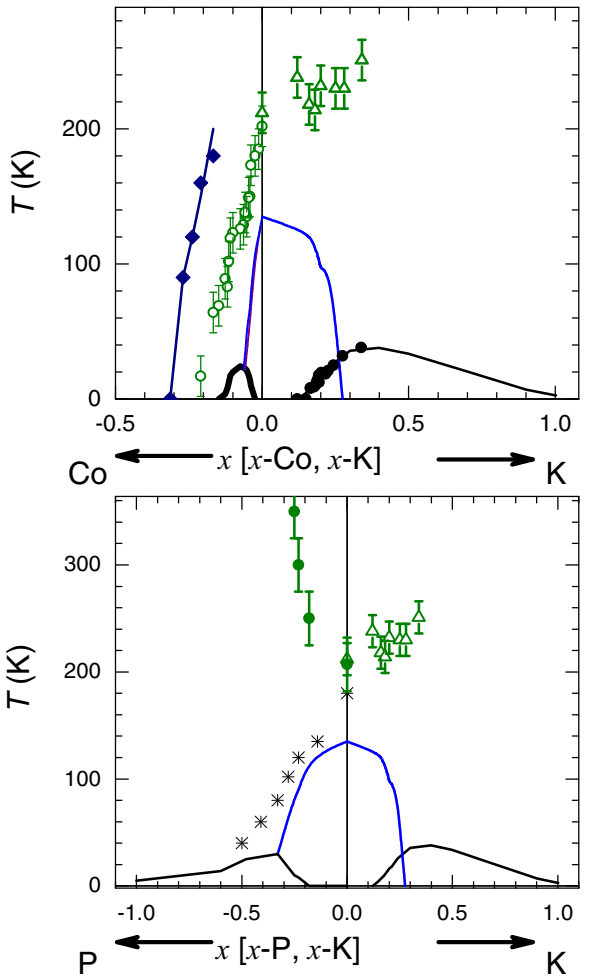

FIG. 5. (Color online) Doping phase diagram of hole-doped $(Ba_{1-x}K_x)Fe_2As_2$ shown in comparison with those of electron-doped $Ba(Fe_{1-x}Co_x)_2As_2$ (top panel) and isoelectron-substituted $BaFe_2(As_{1-x}P_x)_2$ (bottom panel). Lines show the boundaries of orthorhombic (nematic) and magnetically ordered phases and of superconductivity. Open up triangles show T_{max} in BaK122 as found in this study; open and solid circles show the same features in BaCo122 and BaP122; diamonds show the resistivity minimum found in $\rho_c(T)$ in heavily overdoped BaCo122 [18]; stars show the onset temperature of the nematic anomaly in torque measurements in BaP122 [68]. Note the asymmetric evolution of the temperature of the maximum of the interplane resistivity T_{max}, for electron and hole doping and the much faster increase of $T_{max}(x)$ in isoelectron-substituted BaP122 than in hole-doped BaK122.

for different evolution with doping of the resistivity crossover maximum at T_{max}.

B. Maximum of interplane resistivity at T_{max}

It is important to notice that the crossover feature at T_{max} in $\rho_c(T)$ is observed through all compositions from the parent $x = 0$ to 0.34, close to optimal doping. The data of Refs. [59–62] show that the crossover feature is observed even in heavily overdoped KFe_2As_2 ($x = 1$). As can be seen in Fig. 6 below, the slope-change feature in the in-plane resistivity $\rho_a(T)$ at around 200 K shows clear correlation with the crossover maximum in $\rho_c(T)$ at T_{max}. This is true for all doping levels, as can be seen from the comparison of Fig. 3 with data of Ref. [32]. Both these facts strongly argue against an explanation of the maximum as arising from the balance of several contributions to the conductivity. Indeed, the contributions of different sheets of the Fermi surface to the interplane transport are determined by their warping, and those to the in-plane transport by their size. Thus observation of the crossover features at the same temperature on strong variation of the doping level and concomitant changes of the volumes of the electron and hole Fermi-surface sheets [63,64] will invoke superficial selection of combinations of carrier densities and mobilities.

In BaCo122 the decrease of the interplane resistivity above T_{max} shows a clear correlation with the increase of NMR Knight shift. It also shows a clear correlation of the doping range of its existence with the range of the T-linearly

increasing magnetic susceptibility $\chi(T)$. These two observations were the reason for our suggestion of a relation of the resistivity maximum to onset of carrier activation over a pseudogap. At temperatures below T_{max} both the Knight shift and the interplane resistivity in BaCo122 follow the expectations of a metal with temperature-independent density of states. This density of states becomes temperature dependent at $T > T_{max}$. Recently, similar NMR measurements have been undertaken in optimally doped BaK122 [65] and found a Knight shift which is increasing with temperature and a spin-relaxation rate, $1/T_1T$, which decreases with temperature and becomes constant above ~200 K. We need to notice though that the decrease of the interplane resistivity, despite being very small, would be very difficult to explain by only a change of the scattering mechanism. It would require activation of carriers by excitations over the partial gap on the Fermi surface (the pseudogap).

The largest contributions to the interplane transport come from the most warped sheets of the Fermi surface. According to band structure calculations these are located near the Z point of the Brillouin zone, on the Fermi surface with a dominant contribution of the $d_{3z^2-r^2}$ orbital of the iron atom. This band has the weakest nesting and thus should be the least affected by magnetic fluctuations. Density functional theory and dynamical mean-field theory calculations suggest that these bands are least renomalized [66,67], and reveal a correlation pseudogap. This orbital selectivity of the correlation pseudogap may explain why the carrier activation is most clearly observed in the interplane transport. It does not explain, though, why most localized orbitals affect so strongly in-plane transport only in BaK122 and why the pseudogap value, determining the crossover temperature, is not affected by the doping level change.

C. Doping evolution of T_{max}

In Fig. 5 we plot the phase diagram of hole-doped BaK122 in comparison with the phase diagrams of electron-doped BaCo122 [18] and of the isoelectron-substituted BaP122 [14]. We focus on a comparison of the salient features of the temperature-dependent resistivity, a crossover maximum in $\rho_c(T)$ at T_{max} and a nematic feature found in the in-plane resistivity and torque measurements in BaP122 [68]. First, note the electron-hole asymmetry of $T_{max}(x)$. T_{max} is rapidly suppressed with electron doping, paving the way to the appearance of a minimum in $\rho_c(T)$ of heavily doped BaCo122 (diamonds in Fig. 5). T_{max} very slightly increases on doping up to the optimal level in BaK122. Second, note that the $T_{max}(x)$ dependence in the isoelectron-substituted BaP122 is much stronger than that in the hole-doped BaK122. This difference leads to a very different temperature-dependent in-plane and interplane resistivity at optimal doping.

D. Temperature-dependent resistivity at optimal doping

In Fig. 6 we show the temperature-dependent resistivity of hole-doped BaK122 (top panel), isoelectron-substituted BaP122 (middle panel), and electron-doped BaCo122 (bottom panel), all at optimal doping level. Two features of these curves are prominent. First, in all cases the resistivity is close to linear

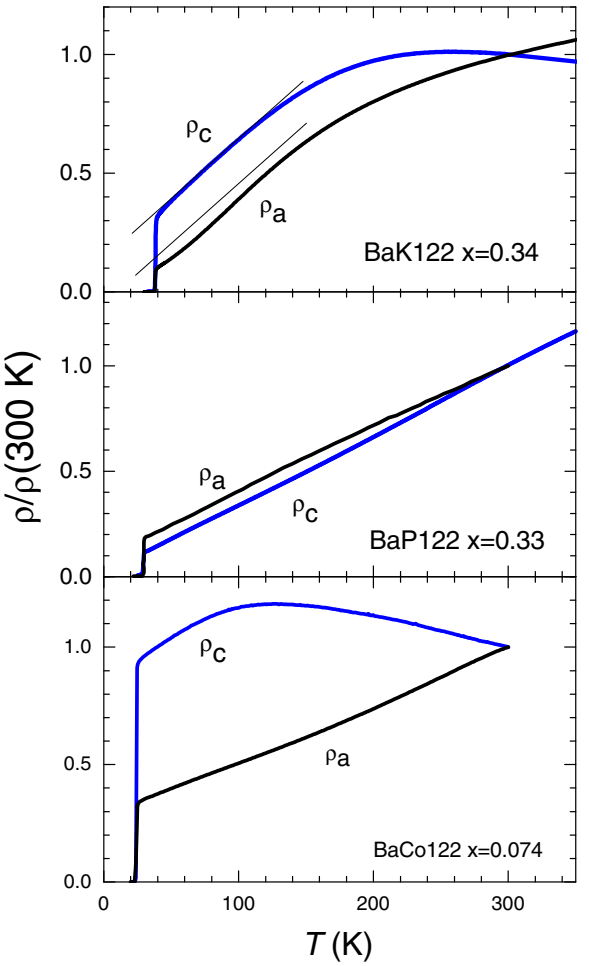

FIG. 6. (Color online) Temperature-dependent in-plane resistivity (black curves) and interplane resistivity (red curves) for samples of hole-doped $(Ba_{1-x}K_x)Fe_2As_2$ (top panel, this study), isoelectron-substituted $BaFe_2(As_{1-x}P_x)_2$ (middle panel, Ref. [14]), and electron-doped $Ba(Fe_{1-x}Co_x)_2As_2$ (bottom panel, Ref. [18]). For all curves the data are normalized by the resistivity values at room temperature $\rho(300)$ K.

in T above T_c. The clearest deviations from linearity are found in $\rho_a(T)$ of BaK122, where some upward curvature can be noticed. This result is similar to previous observations by Shen *et al.* [32]. Interestingly, the interplane resistivity of BaK122 is very close to linear in T, which is reminiscent of the anisotropic T-linear resistivity at the field-tuned quantum critical point of $CeCoIn_5$ [69]. Second, the range of T-linear dependence in many cases is confined from above by a crossover temperature T_{max}. This is particularly clear for the interplane resistivity.

V. CONCLUSIONS

Measurements of the interplane resistivity in BaK122 show that the magnetic/structural transition does not lead to a resistivity increase, i.e., the associated gap does not significantly affect the most warped parts of the Fermi surface, which are important for the interplane transport. Upon suppression of magnetism with doping, the temperature-dependent interplane resistivity reveals T-linear dependence. This occurs close to

the optimal doping just above T_c, suggesting the validity of the QCP scenario. This T-linear behavior persists up to the pseudogap temperature determined by the maximum in ρ_c. As in the electron-doped BaCo122 [18], we assign the origin of this maximum to the activation of carriers over a pseudogap. This pseudogap is indeed found in some band structure calculations taking into account strong electron correlations [66,67], and is particularly pronounced in the Fermi-surface parts with larger contributions from the $d_{3z^2-r^2}$ and $d_{x^2-y^2}$ orbitals. The former is also responsible for the most warped ζ sheet of the KFe_2As_2 Fermi surface [70,71]. This orbital selectivity of the pseudogap may provide a natural explanation as to why the pseudogap feature affects mostly the interplane transport.

Although the effect of doping in multiband metallic systems may be quite complicated, comparison of the hole-doped BaK122 with the electron-doped BaCo122 shows significant differences. The pseudogap resistive crossover at T_{max} in the interplane resistivity vanishes with doping in BaCo122 but remains intact in BaK122. The crossover affects the temperature-dependent in-plane resistivity in BaK122, but not in BaCo122. The pseudogap crossover temperature in BaK122 increases much more slowly than in the isoelectron-substituted BaP122.

Finally we would like to point to a certain similarity in the critical behavior of the interplane resistivity in BaK122 and in $CeCoIn_5$. In $CeCoIn_5$, true critical behavior at a field-tuned QCP [72,73] with T-linear resistivity and violation of the Wiedemann-Franz law is observed for transport along the tetragonal c axis [69], while transport along the plane obeys the Wiedemann-Franz law [74]. This is similar to the difference in the temperature dependence of $\rho_a(T)$ and $\rho_c(T)$ in BaK122, with the latter being more linear at optimal doping.

ACKNOWLEDGMENTS

This work was supported by the U.S. Department of Energy (DOE), Office of Science, Basic Energy Sciences, Materials Science and Engineering Division. The research was performed at the Ames Laboratory, which is operated for the U.S. DOE by Iowa State University under Contract No. DE-AC02-07CH11358. Work in China was supported by the Ministry of Science and Technology of China, Project No. 2011CBA00102. Part of the work done in the University of Sherbrooke was supported by the Canadian Institute for Advanced Research and a Canada Research Chair, and it was funded by NSERC, FQRNT, and CFI.

[1] M. Rotter, M. Tegel, and D. Johrendt, Phys. Rev. Lett. **101**, 107006 (2008).
[2] Y. Kamihara, T. Watanabe, M. Hirano, and H. Hosono, J. Am. Chem. Soc. **130**, 3296 (2008).
[3] C. Kant, J. Deisenhofer, A. Gunther, F. Schrettle, A. Loidl, M. Rotter, and D. Johrendt, Phys. Rev. B **81**, 014529 (2010).
[4] S. Avci, O. Chmaissem, E. A. Goremychkin, S. Rosenkranz, J.-P. Castellan, D. Y. Chung, I. S. Todorov, J. A. Schlueter, H. Claus, M. G. Kanatzidis, A. Daoud-Aladine, D. Khalyavin, and R. Osborn, Phys. Rev. B **83**, 172503 (2011).
[5] S. Avci, O. Chmaissem, D. Y. Chung, S. Rosenkranz, E. A. Goremychkin, J. P. Castellan, I. S. Todorov, J. A. Schlueter, H. Claus, A. Daoud-Aladine, D. D. Khalyavin, M. G. Kanatzidis, and R. Osborn, Phys. Rev. B **85**, 184507 (2012).
[6] Sergey L. Bud'ko, Mihai Sturza, Duck Young Chung, Mercouri G. Kanatzidis, and Paul C. Canfield, Phys. Rev. B **87**, 100509 (2013).
[7] P. C. Canfield and S. L. Bud'ko, Annu. Rev. Condens. Matter Phys. **1**, 27 (2010).
[8] S. Kasahara, T. Shibauchi, K. Hashimoto, K. Ikada, S. Tonegawa, R. Okazaki, H. Shishido, H. Ikeda, H. Takeya, K. Hirata, T. Terashima, and Y. Matsuda, Phys. Rev. B **81**, 184519 (2010).
[9] N. Doiron-Leyraud, P. Auban-Senzier, S. Renéde Cotret, C. Bourbonnais, D. Jérome, K. Bechgaard, and L. Taillefer, Phys. Rev. B **80**, 214531 (2009).
[10] Y. Nakai, T. Iye, S. Kitagawa, K. Ishida, H. Ikeda, S. Kasahara, H. Shishido, T. Shibauchi, Y. Matsuda, and T. Terashima, Phys. Rev. Lett. **105**, 107003 (2010).
[11] P. Monthoux, D. Pines, and G. G. Lonzarich, Nature (London) **450**, 1177 (2007).
[12] M. R. Norman, Science **332**, 196 (2011).
[13] Louis Taillefer, Annu. Rev. Condens. Matter Phys. **1**, 51 (2010).
[14] M. A. Tanatar, K. Hashimoto, S. Kasahara, T. Shibauchi, Y. Matsuda, and R. Prozorov, Phys. Rev. B **87**, 104506 (2013).
[15] K. Hashimoto, K. Cho, T. Shibauchi, S. Kasahara, Y. Mizukami, R. Katsumata, Y. Tsuruhara, T. Terashima, H. Ikeda, M. A. Tanatar, H. Kitano, N. Salovich, R. W. Giannetta, P. Walmsley, A. Carrington, R. Prozorov, and Y. Matsuda, Science **336**, 1554 (2012).
[16] S. Nandi, M. G. Kim, A. Kreyssig, R. M. Fernandes, D. K. Pratt, A. Thaler, N. Ni, S. L. Budko, P. C. Canfield, J. Schmalian, R. J. McQueeney, and A. I. Goldman, Phys. Rev. Lett. **104**, 057006 (2010).
[17] M. A. Tanatar, N. Ni, C. Martin, R. T. Gordon, H. Kim, V. G. Kogan, G. D. Samolyuk, S. L. Bud'ko, P. C. Canfield, and R. Prozorov, Phys. Rev. B **79**, 094507 (2009).
[18] M. A. Tanatar, N. Ni, A. Thaler, S. L. Bud'ko, P. C. Canfield, and R. Prozorov, Phys. Rev. B **82**, 134528 (2010).
[19] M. A. Tanatar, N. Ni, A. Thaler, S. L. Bud'ko, P. C. Canfield, and R. Prozorov, Phys. Rev. B **84**, 014519 (2011).
[20] F. L. Ning, K. Ahilan, T. Imai, A. S. Sefat, R. Jin, M. A. McGuire, B. C. Sales, and D. Mandrus, J. Phys. Soc. Jpn. **77**, 103705 (2008).
[21] F. L. Ning, K. Ahilan, T. Imai, A. S. Sefat, M. A. McGuire, B. C. Sales, D. Mandrus, P. Cheng, B. Shen, and H.-H. Wen, Phys. Rev. Lett. **104**, 037001 (2010).
[22] S. J. Moon, A. A. Schafgans, S. Kasahara, T. Shibauchi, T. Terashima, Y. Matsuda, M. A. Tanatar, R. Prozorov, A. Thaler, P. C. Canfield, A. S. Sefat, D. Mandrus, and D. N. Basov, Phys. Rev. Lett. **109**, 027006 (2012).

[23] S. J. Moon, A. A. Schafgans, M. A. Tanatar, R. Prozorov, A. Thaler, P. C. Canfield, A. S. Sefat, D. Mandrus, and D. N. Basov, Phys. Rev. Lett. **110**, 097003 (2013).
[24] T. Shimojima *et al.*, Phys. Rev. B **89**, 045101 (2014).
[25] T. Timusk and B. Statt, Rep. Prog. Phys. **62**, 61 (1999).
[26] N. P. Armitage, P. Fournier, and R. L. Greene, Rev. Mod. Phys. **82**, 2421 (2010).
[27] N. Doiron-Leyraud and Louis Taillefer, Physica C **481**, 161 (2012).
[28] R. Daou, J. Chang, David LeBoeuf, Olivier Cyr-Choiniere, Francis Laliberte, Nicolas Doiron-Leyraud, B. J. Ramshaw, Ruixing Liang, D. A. Bonn, W. N. Hardy, and Louis Taillefer, Nature (London) **463**, 512 (2010).
[29] R. M. Fernandes, A. V. Chubukov, and J. Schmalian, Nat. Phys. **10**, 97 (2014).
[30] E. C. Blomberg, M. A. Tanatar, R. M. Fernandes, I. I. Mazin, B. Shen, H.-H. Wen, M. D. Johannes, J. Schmalian, and R. Prozorov, Nat. Commun. **4**, 1914 (2013).
[31] H. Q. Luo, Z. S. Wang, H. Yang, P. Cheng, X. Zhu, and H.-H. Wen, Supercond. Sci. Technol. **21**, 125014 (2008).
[32] Bing Shen, Huan Yang, Zhao-Sheng Wang, Fei Han, Bin Zeng, Lei Shan, Cong Ren, and Hai-Hu Wen, Phys. Rev. B **84**, 184512 (2011).
[33] Y. M. Dai, B. Xu, B. Shen, H. Xiao, H. H. Wen, X. G. Qiu, C. C. Homes, and R. P. S. M. Lobo, Phys. Rev. Lett. **111**, 117001 (2013).
[34] A. A. Golubov, O. V. Dolgov, A. V. Boris, A. Charnukha, D. L. Sun, C. T. Lin, A. F. Shevchun, A. V. Korobenko, M. R. Trunin, and V. N. Zverev, JETP Lett. **94**, 333 (2011).
[35] V. A. Gasparov, F. Wolff-Fabris, D. L. Sun, C. T. Lin, and J. Wosnitza, JETP Lett. **93**, 26 (2011).
[36] E. Hassinger, G. Gredat, F. Valade, S. R. deCotret, A. Juneau-Fecteau, J.-Ph. Reid, H. Kim, M. A. Tanatar, R. Prozorov, B. Shen, H.-H. Wen, N. Doiron-Leyraud, and L. Taillefer, Phys. Rev. B **86**, 140502 (2012).
[37] S. Avci, J. M. Allred, O. Chmaissem, D. Y. Chung, S. Rosenkranz, J. A. Schlueter, H. Claus, A. Daoud-Aladine, D. D. Khalyavin, P. Manuel, A. Llobet, M. R. Suchomel, M. G. Kanatzidis, and R. Osborn, Phys. Rev. B **88**, 094510 (2013).
[38] N. Ni, S. L. Bud'ko, A. Kreyssig, S. Nandi, G. E. Rustan, A. I. Goldman, S. Gupta, J. D. Corbett, A. Kracher, and P. C. Canfield, Phys. Rev. B **78**, 014507 (2008).
[39] Sutirtha Mukhopadhyay, Sangwon Oh, A. M. Mounce, Moohee Lee, W. P. Halperin, N. Ni, S. L. Bud'ko, P. C. Canfield, A. P. Reyes, and P. L. Kuhns, New J. Phys. **11**, 055002 (2009).
[40] M. A. Tanatar, N. Spyrison, Kyuil Cho, E. C. Blomberg, Guotai Tan, Pengcheng Dai, Chenglin Zhang, and R. Prozorov, Phys. Rev. B **85**, 014510 (2012).
[41] N. Spyrison, M. A. Tanatar, Kyuil Cho, Y. Song, Pengcheng Dai, Chenglin Zhang, and R. Prozorov, Phys. Rev. B **86**, 144528 (2012).
[42] R. Prozorov, N. Ni, M. A. Tanatar, V. G. Kogan, R. T. Gordon, C. Martin, E. C. Blomberg, P. Prommapan, J. Q. Yan, S. L. Bud'ko, and P. C. Canfield, Phys. Rev. B **78**, 224506 (2008).
[43] R. Prozorov, M. A. Tanatar, B. Roy, N. Ni, S. L. Bud'ko, P. C. Canfield, J. Hua, U. Welp, and W. K. Kwok, Phys. Rev. B **81**, 094509 (2010).
[44] M. A. Tanatar, N. Ni, S. L. Bud'ko, P. C. Canfield, and R. Prozorov, Supercond. Sci. Technol. **23**, 054002 (2010).
[45] M. A. Tanatar, R. Prozorov, N. Ni, S. L. Bud'ko, and P. C. Canfield, U. S. Patent No. 8,450,246 (Sept. 1, 2011).
[46] M. A. Tanatar, N. Ni, G. D. Samolyuk, S. L. Bud'ko, P. C. Canfield, and R. Prozorov, Phys. Rev. B **79**, 134528 (2009).
[47] M. R. Presland, J. L. Tallon, R. G. Buckley, R. S. Liu, and N. E. Flower, Physica C **176**, 95 (1991).
[48] J. Paglione and R. L. Greene, Nat. Phys. **6**, 645 (2010).
[49] D. C. Johnston, Adv. Phys. **59**, 803 (2010).
[50] G. R. Stewart, Rev. Mod. Phys. **83**, 1589 (2011).
[51] E. Colombier, S. L. Bud'ko, N. Ni, and P. C. Canfield, Phys. Rev. B **79**, 224518 (2009).
[52] S. K. Kim, M. S. Torikachvili, E. Colombier, A. Thaler, S. L. Bud'ko, and P. C. Canfield, Phys. Rev. B **84**, 134525 (2011).
[53] Takayoshi Katase, Hikaru Sato, Hidenori Hiramatsu, Toshio Kamiya, and Hideo Hosono, Phys. Rev. B **88**, 140503 (2013).
[54] I. I. Mazin and M. D. Johannes, Nat. Phys. **5**, 141 (2009); M. D. Johannes and I. I. Mazin, Phys. Rev. B **79**, 220510 (2009).
[55] Lei Fang, Huiqian Luo, Peng Cheng, Zhaosheng Wang, Ying Jia, Gang Mu, Bing Shen, I. I. Mazin, Lei Shan, Cong Ren, and Hai-Hu Wen, Phys. Rev. B **80**, 140508(R) (2009).
[56] F. Rullier-Albenque, D. Colson, A. Forget, and H. Alloul, Phys. Rev. Lett. **103**, 057001 (2009).
[57] M. A. Tanatar, E. C. Blomberg, A. Kreyssig, M. G. Kim, N. Ni, A. Thaler, S. L. Bud'ko, P. C. Canfield, A. I. Goldman, I. I. Mazin, and R. Prozorov, Phys. Rev. B **81**, 184508 (2010).
[58] Taichi Terashima, Nobuyuki Kurita, Megumi Tomita, Kunihiro Kihou, Chul-Ho Lee, Yasuhide Tomioka, Toshimitsu Ito, Akira Iyo, Hiroshi Eisaki, Tian Liang, Masamichi Nakajima, Shigeyuki Ishida, Shin-ichi Uchida, Hisatomo Harima, and Shinya Uji, Phys. Rev. Lett. **107**, 176402 (2011).
[59] Taichi Terashima, Motoi Kimata, Hidetaka Satsukawa, Atsushi Harada, Kaori Hazama, Shinya Uji, Hisatomo Harima, Gen-Fu Chen, Jian-Lin Luo, and Nan-Ling Wang, J. Phys. Soc. Jpn. **78**, 063702 (2009).
[60] M. Kimata, T. Terashima, N. Kurita, H. Satsukawa, A. Harada, K. Kodama, A. Sato, M. Imai, K. Kihou, C. H. Lee, H. Kito, H. Eisaki, A. Iyo, T. Saito, H. Fukazawa, Y. Kohori, H. Harima, and S. Uji, Phys. Rev. Lett. **105**, 246403 (2010).
[61] J.-Ph. Reid, M. A. Tanatar, A. Juneau-Fecteau, R. T. Gordon, S. R. de Cotret, N. Doiron-Leyraud, T. Saito, H. Fukazawa, Y. Kohori, K. Kihou, C. H. Lee, A. Iyo, H. Eisaki, R. Prozorov, and L. Taillefer, Phys. Rev. Lett. **109**, 087001 (2012).
[62] Yong Liu, M. A. Tanatar, V. G. Kogan, Hyunsoo Kim, T. A. Lograsso, and R. Prozorov, Phys. Rev. B **87**, 134513 (2013).
[63] K. Nakayama, T. Sato, P. Richard, Y.-M. Xu, T. Kawahara, K. Umezawa, T. Qian, M. Neupane, G. F. Chen, H. Ding, and T. Takahashi, Phys. Rev. B **83**, 020501(R) (2011).
[64] T. Yoshida, I. Nishi, S. Ideta, A. Fujimori, M. Kubota, K. Ono, S. Kasahara, T. Shibauchi, T. Terashima, Y. Matsuda, H. Ikeda, and R. Arita, Phys. Rev. Lett. **106**, 117001 (2011).
[65] Z. Li, D. L. Sun, C. T. Lin, Y. H. Su, J. P. Hu, and G.-q. Zheng, Phys. Rev. B **83**, 140506 (2011).
[66] M. Aichhorn, S. Biermann, T. Miyake, A. Georges, and M. Imada, Phys. Rev. B **82**, 064504 (2010).
[67] Ph. Werner, M. Casula, T. Miyake, F. Aryasetiawan, A. J. Millis, and S. Biermann, Nat. Phys. **8**, 331 (2012).
[68] S. Kasahara, H. J. Shi, K. Hashimoto, S. Tonegawa, Y. Mizukami, T. Shibauchi, K. Sugimoto, T. Fukuda, T. Terashima,

Andriy H. Nevidomskyy, and Y. Matsuda, Nature (London) **486**, 382 (2012).

[69] M. A. Tanatar, J. Paglione, C. Petrovic, and L. Taillefer, Science **316**, 1320 (2007).

[70] Taichi Terashima, Nobuyuki Kurita, Motoi Kimata, Megumi Tomita, Satoshi Tsuchiya, Motoharu Imai, Akira Sato, Kunihiro Kihou, Chul-Ho Lee, Hijiri Kito, Hiroshi Eisaki, Akira Iyo, Taku Saito, Hideto Fukazawa, Yoh Kohori, Hisatomo Harima, and Shinya Uji, Phys. Rev. B **87**, 224512 (2013).

[71] T. Yoshida, S.-I. Ideta, I. Nishi, A. Fujimori, M. Yi, R. G. Moore, S.-K. Mo, D. Lu, Z.-X. Shen, Z. Hussain, K. Kihou, P. M. Shirage, H. Kito, C.-H. Lee, A. Iyo, H. Eisaki, and H. Harima, Fron. Physics. Cond-Matt. Phys. **2**, 17 (2014).

[72] Johnpierre Paglione, M. A. Tanatar, D. G. Hawthorn, Etienne Boaknin, R. W. Hill, F. Ronning, M. Sutherland, Louis Taillefer, C. Petrovic, and P. C. Canfield, Phys. Rev. Lett. **91**, 246405 (2003).

[73] A. Bianchi, R. Movshovich, I. Vekhter, P. G. Pagliuso, and J. L. Sarrao, Phys. Rev. Lett. **91**, 257001 (2003).

[74] Johnpierre Paglione, M. A. Tanatar, D. G. Hawthorn, F. Ronning, R. W. Hill, M. Sutherland, Louis Taillefer, and C. Petrovic, Phys. Rev. Lett. **97**, 106606 (2006).